Macromolecules

Article

Cite This: Macromolecules 2017, 50, 8202-8211

pubs.acs.org/Macromolecules

Tuning DNA Condensation with Zwitterionic Polyamidoamine (zPAMAM) Dendrimers

Min An,[†] Gulen Yesilbag Tonga,[‡] Sean R. Parkin,[†] Vincent M. Rotello,[‡] and Jason E. DeRouchey*[,†]

[†]Department of Chemistry, University of Kentucky, Lexington, Kentucky 40506, United States

[‡]Department of Chemistry, University of Massachusetts Amherst, Amherst, Massachusetts 01003, United States

Supporting Information

ABSTRACT: Cationic dendrimers are promising vectors for nonviral gene therapies due to their well-defined size and chemistry. We have synthesized a series of succinylated fourth generation (G4) PAMAM dendrimers to control the DNA packaging in dendriplexes, allowing us to probe the role of charge on DNA packaging. The self-assembly of DNA induced by these zwitterionic PAMAM (zPAMAM) was investigated using small-angle X-ray scattering (SAXS). We demonstrate that changing the degree of modification in zPAMAM−DNA significantly alters the packing density of the resulting dendriplexes. Salt sensitivities and pH dependence on the inter-DNA spacing were also examined. The swelling and stability to salt are reduced with increasing degree of PAMAM modification. Lowering the pH leads to significantly tighter hexagonal DNA packaging. In combination, these results show zPAMAM is an effective means to modulate nucleic acid packaging in a deterministic manner.

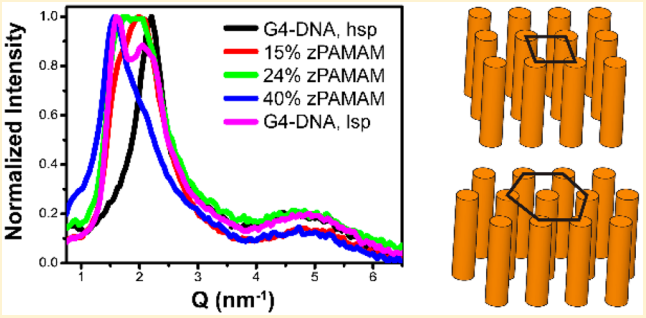

INTRODUCTION

Complexation of nucleic acids with polycations is relevant to *in vivo* DNA packaging as well as for nonviral gene delivery. In eukaryote nuclei, cationic nuclear proteins including histones, protamines, and biogeneic polyamines, such as spermine and spermidine, condense DNA.[1−3] Beyond DNA compaction, experiments also show DNA condensation likely serves as a regulatory mechanism of gene expression in cells.[4,5] In nonviral gene delivery, extracellular DNA is typically complexed by cationic lipids or synthetic polymers to create supramolecular complexes that are readily endocytosed into cells and ultimately transcribed.[6,7] In both cases, spontaneous assembly of the DNA molecules is primarily driven by electrostatic interactions with the cationic species and the entropic gains resulting from counterion release.[8−10] Polycation−DNA complexes (polyplexes) represent a particularly attractive approach to nonviral DNA delivery carriers due to their low immunogenicity and ease of chemical modification.[11−13]

Dendrimers are highly symmetrical branched macromolecules with precisely defined size, molecular weight, and surface chemistries—a distinct advantage over synthetic linear polymers for control of polyplex assembly. Cationic dendrimers have therefore become attractive alternatives to traditional linear polycationic systems for nucleic acid delivery. Typically, dendrimers are built in an iterative fashion with concentric branching units stemming from a central core. With each growth step, or generation, a doubling of the reactive surface groups is achieved. The commercially available cationic dendrimers poly(amidoamine) (PAMAM) and polypropyleneimine (PPI) represent the most studied dendrimer−DNA, or dendriplex systems.[14,15] Both dendrimers have been shown capable of condensing DNA and protecting nucleic acids from restriction nucleases. Despite the extensive use of dendrimers as a gene delivery agent, the role of charge in determining the efficiency and morphology of compaction and the stability of the resulting complexes is not well understood.

To date, a wide variety of structures that depend on the dendrimer chemistry and generation have been reported for dendriplexes. One of the first structural studies of dendriplexes showed that DNA condensed by G4 and G5 PPI self-assembles to form polymorphic hexagonal or square columnar mesophases.[16] Subsequent studies by small-angle X-ray scattering (SAXS) have shown in-plane square and hexagonal symmetries, bead-on-a-string morphologies, and coexistence between phases for intermediate generation (∼G3−G6) PAMAM and PPI dendriplexes.[16−29] In contrast, DNA condensed by low generations dendrimers (∼G0−G2) typically gives hexagonal phases comparable to linear cationic systems,[20−22,25,26] and high generation dendrimers (>G6) are generally observed to form disordered globules or DNA wrapped structures.[21,29] Recent work has shown that the supramolecular structure of the dendriplex can strongly impact the resulting cellular uptake and gene transfection efficiency.[21,30−32] Functionalization of the dendrimer surface groups, such as acetylation, is also known to

Received: July 11, 2017
Revised: September 8, 2017
Published: October 9, 2017

DOI: 10.1021/acs.macromol.7b01470
Macromolecules 2017, 50, 8202−8211

alter significantly the efficiency of nucleic acid delivery in cells presumably by altering the dendrimer−DNA interaction strength that controls DNA release from such dendriplexes.[21,33]

A key challenge for developing new transfection agents, however, is how to effectively control the resulting morphology and stabilities of the dendriplex gene delivery agents.

In the present study, we investigate the internal structure of dendriplexes resulting from the condensation of DNA with modified zwitterionic G4-PAMAM (zPAMAM) polymers. We hypothesized that tuning the charge of the dendrimer system through succinylation of the surface functional amines would be a means to engineer the resulting DNA−dendrimer interactions. zPAMAM with varying degrees of succinylation (0−40%) were synthesized and found capable of inducing DNA condensation. SAXS experiments were performed to determine the self-assembled morphologies of the condensed zPAMAM dendriplexes. Inter-DNA spacings as a function of percent zwitterion modification are compared to unmodified G4-PAMAM/DNA condensates using both a low and high salt preparation method. We show that the high salt method is a means to overcome nonequilibrium states observed in dendriplexes condensed at low salt. With increasing degree of succinylation in zPAMAM−DNA, significant structural rearrangements were observed. Incorporation of negative charges on the PAMAM molecule reduces the dendrimer−DNA interactions inducing a systematic phase transition from a tightly packaged hexagonal phase to a more loosely ordered square phase. Salt studies were performed to assess the resulting zPAMAM dendriplex stabilities. Lastly, we show that lowering the pH increases the ionic interaction, resulting in significantly tighter packaging in both G4 and zPAMAM condensates.

EXPERIMENTAL SECTION

Materials. High-molecular-weight DNA (MW > 5×10^6 Da) was prepared and purified from adult-chicken whole blood as described previously[34] and dialyzed against 10 mM TrisCl (pH 7.5) and 1 mM EDTA. After purification, DNA was extensively dialyzed against 1 mM EDTA solution. Successful removal of protein from the DNA was verified by measuring the ratio of absorbance at 260 and 280 nm of DNA solutions and found to be satisfactory with values exceeding 1.8. PAMAM dendrimer (ethylenediamine core, generation 4.0 solution in 10% methanol) was purchased from Sigma-Aldrich (St. Louis, MO). NaN_3, HCl, NaOH, and sodium acetate were purchased from Sigma. 2-(*N*-Morpholino)ethanesulfonic acid (MES) buffer and EDTA were purchased from Fisher. 1 M Tris pH 7.5 buffer was purchased from Mediatech Inc. All chemicals were used without further purification.

Synthesis of zPAMAM. PAMAM G4 dendrimer (in methanol, 10 wt %) was reacted with the desired mole ratio of succinic anhydride in dimethylformamide (DMF) after evaporating the methanol. The succinylation reaction proceeded for 15 h at room temperature, and the final product, zPAMAM, was purified by dialysis (membrane molecular weight cutoff = 10 000). After dialysis, the solution was filtered once through a molecular-weight cutoff filter (Millex GP, Millipore, PES membrane, 0.22 μm) and then lyophilized to yield a solid white product. Percent succinylation was determined by ^{1}H NMR in D_2O. Three zwitterionic PAMAMs (zPAMAM) were synthesized and used in this study: 15%, 24%, and 40% succinylation modification of the PAMAM primary surface groups.

Sample Preparation. DNA dendriplexes were prepared from mixtures of purified chicken blood (CB) DNA with either unmodified or zwitterionic PAMAM. In preparing samples, both the DNA and G4-PAMAM dendrimer stock solutions were first separately dissolved in an appropriate 10 mM pH buffer. After dissolution, these stock solutions were further buffered with HCl or NaOH to achieve the desired final pH (pH ± 0.1). Buffers used were 10 mM sodium acetate solution for pH 4, 10 mM MES solution for pH 6, and 10 mM Tris-HCl for pH 8 and pH 7.5. The double-helix structure of DNA is known to be stable over this pH range. In this work, we used two different methods for the preparation of PAMAM/DNA samples for analysis by X-rays. We will refer to these methods as low salt preparation (lsp) and high salt preparation (hsp), each resulting in fibrous dendriplex samples suitable for X-ray analysis. For both high and low salt preparations, ∼250 μg of CB DNA was used per X-ray sample. In the low salt preparation (lsp) method, concentrated PAMAM or zPAMAM stock solutions were added to 1 mg/mL CB DNA in 10 mM pH buffer in a stepwise fashion. Each addition was mixed thoroughly before adding additional dendrimer, and the process continued until all DNA was precipitated. The resulting fibrous dendriplex complex was then equilibrated in a bathing solution of 10 mM pH buffer. Alternatively, in the high salt preparation (hsp), DNA and the chosen polycation were dissolved separately in a 2 M NaCl salt solution with the appropriate pH buffer. Based upon the required PAMAM or zPAMAM to condense all the DNA observed in the low salt preparation, a sufficient amount of dendrimer was added to the DNA to ensure complete condensation. Solutions were then mixed and allowed to equilibrate for approximately 30 min. The high salt concentration prevents condensation from occurring and allows thorough mixing of the dendrimer and DNA in the solution. Precipitation was subsequently induced by dilution with additional buffer solution, resulting in a solid fibrous condensate. This condensate was collected by centrifugation (10000*g*/10 min) and washed repeatedly with buffer to extract as much salt as possible. The condensate was then moved to a bathing solution of 10 mM pH buffer solution to equilibrate. As discussed in the Results section, the hsp method was found to make stable dendriplexes that do not show significant internal structure rearrangements over several months. Unless otherwise stated, all fibrous PAMAM−DNA samples were transferred to the desired buffered solution and allowed to equilibrate for 2 weeks before X-ray analysis. In all samples, a small excess dendrimer concentration (∼0.1 μM) was maintained in the bathing solution to ensure cation concentration was above the critical concentration. The observed DNA−DNA spacings in G4 and zPAMAM dendriplexes were not dependent on the excess cation concentration in the bath over a 2-fold concentration range.

Small-Angle X-ray Scattering (SAXS). Graded-multilayer focused Cu Kα (λ = 1.54 Å) radiation from a Nonius FR-591 rotating anode fine-focus X-ray generator operating at 45 kV and 20 mA was used for the SAXS experiments. The primary beam was collimated using a fine rear aperture beam tunnel. Samples were sealed with a bath of equilibrating solution in the sample cell and then mounted into a custom sample holder at room temperature (∼21 °C). The flight path between the sample and the detector was filled with helium to minimize background scatter. Diffraction patterns were recorded with a Bruker SMART 6000 CCD detector, with phosphor optimized for Cu Kα radiation. Images were analyzed with Fit2d and Origin 8.0 software. Calibration of the SAXS sample-to-detector distance was performed using silver behenate powder and found to be 23.2 cm. The electron density of DNA is significantly larger than the electron density of dendrimer or water and thus dominates the observed scattering profiles. Bragg scattering peaks were used to determine interaxial DNA−DNA spacings. Bragg spacings, which corresponds to the maximum in the scattering, are calculated as $D_{Bragg} = 2\pi/q_{Br}$, where q_{Br} is the scattering vector, q (defined as $q = (4\pi/\lambda)\sin(\theta)$, where 2θ is the scattering angle). For a hexagonal lattice, the relationship between the Bragg spacing and the actual interaxial distance between DNA helices (D_{int}) is calculated as $D_{int} = (2/\sqrt{3})D_{Bragg}$. For different samples equilibrated under the same buffered conditions, D_{int} values were reproducible to within ∼0.1 Å. There was no significant sample degradation due to X-ray exposure. Typical exposure times were 120 s.

RESULTS AND DISCUSSION

Synthesis and Characterization of zPAMAM. To explore the effects of zwitterionic character on dendrimer−DNA structure, we modified commercially available G4-

DOI: 10.1021/acs.macromol.7b01470
Macromolecules 2017, 50, 8202−8211

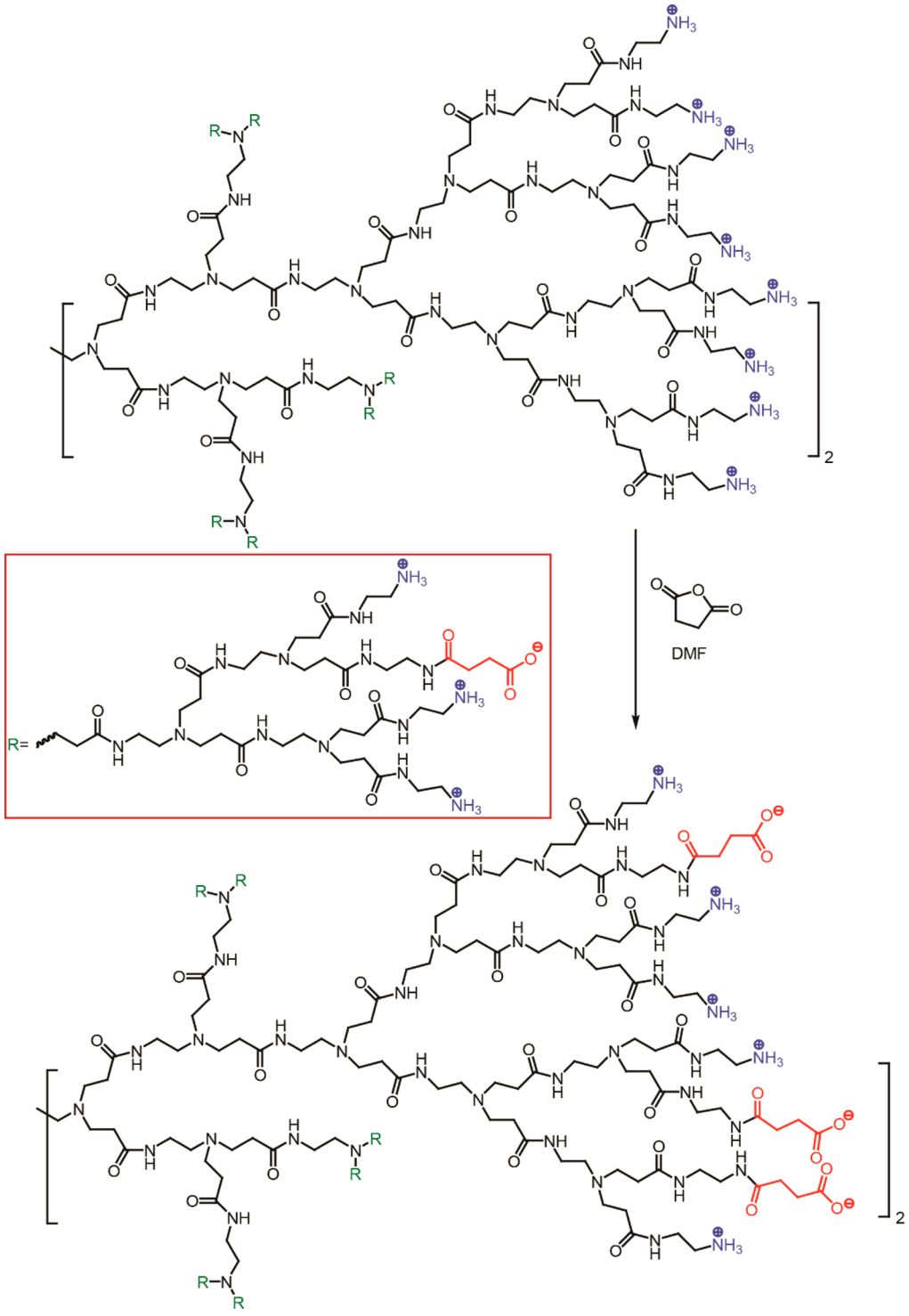

Figure 1. Synthesis scheme for zwitterionic PAMAM (zPAMAM). Dendrimers with varying percentage of zwitterionic functionality were synthesized by reacting PAMAM G4 dendrimers with succinic anhydride in DMF for 15 h at room temperature. NMR spectra were analyzed to calculate the degree of functionalization.

PAMAM (G4) with succinic anhydride to create a series of zwitterionic PAMAM (zPAMAM) polymers (Figure 1). G4 was reacted with differing amounts of succinic anhydride in DMF for 15 h at room temperature. Only the primary amines located on the terminal ends of the PAMAM will react with anhydride to convert some surface amines to carboxylic acid groups. Reaction products were subsequently purified by dialysis and filtered through a 0.22 μm filter and then lyophilized. The extent of succinylation was determined by ^{1}H NMR spectroscopy (Figures S1−S3). After succinylation reaction, integration of the peak at around 2.3 ppm increased, while the peak at 2.58 ppm in nonfunctionalized PAMAM disappeared. Also, new peaks at around 3.3, 3, and 2.8 ppm appeared in the NMR spectrum. The reactions produced zPAMAM of 15%, 24%, and 40% of the primary functional amines succinylated. As discussed below, all three polymers were observed to induce

DOI: 10.1021/acs.macromol.7b01470
Macromolecules 2017, 50, 8202−8211

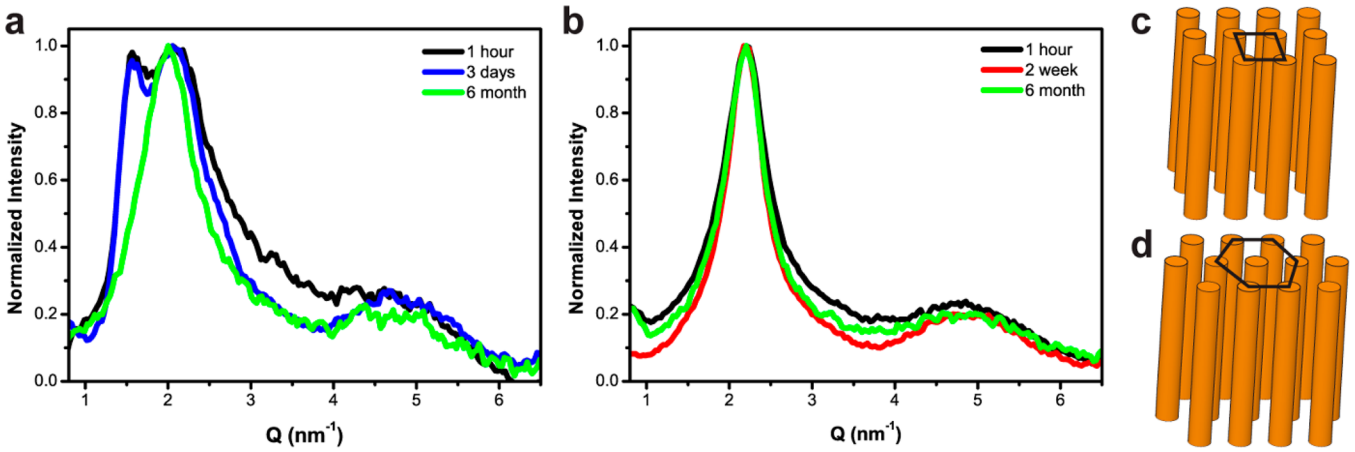

Figure 2. Evolution of G4-PAMAM/DNA assembly structure with time. Representative scattering profiles for DNA condensed by G4-PAMAM using (a) low and (b) high salt preparation in 10 mM Tris (pH 7.5). Plotted is the normalized intensity (I/I_{max}) as a function of the scattering vector Q. The low salt preparation results in coexistence of two ordered columnar DNA phases consistent with a columnar square lattice (c) and columnar hexagonal lattice (d). Over several months, the samples significantly reorganize to form only the hexagonal lattice. High salt preparation results in only the hexagonal lattice with the same Bragg spacing being observed with no significant rearrangements over several months.

DNA condensation. Dynamic light scattering experiments (Malvern Zetasizer) showed no significant aggregation upon succinylation of the PAMAM molecules. However, by DLS, we cannot rule out the presence of some amount of small aggregates (e.g., dimers and trimers) which have recently been shown to be present in commercial biomedical grade PAMAM.[35]

Stability of G4-PAMAM/DNA Assemblies Condensed under Low and High Salt Conditions. *In vitro* it has been shown that DNA can spontaneously self-assemble in the presence of cations with charge of +3 or higher.[36] For linear cations, DNA is typically arranged in a hexagonal lattice with helices lying parallel to one another with well-defined equilibrium surface separations. The finite separation of the DNA is a result of a balancing of the short-range repulsive forces and long-range attraction in the system.[37,38] X-ray scattering experiments allow measurement of the inter-DNA spacings in the DNA condensed phase. Depending on cation chemistry, observed surface separations typically range from 7 to 12 Å of water between DNA surfaces.[39−42]

In contrast to typical polyplexes, a wide variety of structures and spacings have been described previously for dendriplexes. Depending on the dendrimer chemistry, generation, and mixing ratios, square and hexagonally columnar mesophases, DNA wrapping, and coexistence between phases have all been reported for intermediate generation dendrimers. Transmission electron microscopy (TEM) studies have shown both low and intermediate generation dendriplexes generally form toroidal and rod shaped nanoparticles.[21] Rod and toroidal aggregates are commonly reported in linear cation/DNA condensates *in vitro*.[43,44] Toroids with in-plane hexagonal packaging of the DNA are also known to occur *in vivo* in sperm chromatin.[45] The spherical shape and geometric size of intermediate and high generation dendrimers are of the order of histone proteins and were theoretically predicted to result in DNA wrapping or bead on a string (BOS).[46,47] The formation of BOS structures is generally observed in dilute conditions and results from a balance of electrostatic attraction and the energy cost of bending the rigid DNA helix. Even for the same G4 PAMAM dendrimer system, this polymorphism has been observed, however, with some variation in the assigned structure and DNA spacings reported.[17,22,23,27,48] Therefore, before demonstrating the effects of zPAMAM on the dendriplex structure, we first examined the resulting structure of DNA complexed by unmodified G4 PAMAM (G4) dendrimer.

Here, concentrated DNA solutions are condensed with PAMAM using either a low salt preparation (lsp) or high salt preparation (hsp) method at near neutral pH. Both methods result in a fibrous sample suitable for X-ray analysis. In lsp, both the DNA and PAMAM were dissolved in 10 mM Tris buffer (pH 7.5). Sufficient dendrimer was added to the DNA solution to fully condense the DNA; typically, total nitrogen to phosphate (N/P) ratios of 2−10 were used for all PAMAM and zPAMAM systems discussed in this work. After complete condensation, free DNA in the supernatant was negligible as determined by UV−vis. The resulting fibrous samples were then transferred to ∼1 mL of a bathing solution of 10 μM Tris (pH 7.5), 0.4 mM NaN_3, and 0.1 μM excess dendrimer and equilibrated. Bathing solutions were changed two times during equilibration. Sodium azide was added to inhibit microbial growth and was not observed to have any effect on the measured DNA spacings. A slight excess of dendrimer was added to maintain a cation concentration slightly above the critical concentration to alleviate concerns of potential leeching of the condensing agent from the fibrous condensate. Incubating with 2-fold change (50 or 200 nM excess dendrimer) in the bathing solution did not affect the interhelical spacings. Previously, we observed the DNA−DNA spacings experimentally observed in these fibrous samples for a wide variety of common polyplex formulations were in reasonable agreement with the inter-DNA spacings observed in the corresponding colloidal nanoparticles generated for gene delivery applications.[40] For the hsp method, PAMAM and DNA are first dissolved in buffered 2 M NaCl before mixing the polymer with DNA. The high salt prevents condensation from occurring, thereby allowing for a thorough mixing of the polyelectrolytes. Condensation is subsequently induced by diluting the sample with 10 mM buffer to achieve a lower total salt concentration. Fibrous samples are then thoroughly washed to remove excess salt and placed in a bathing solution of 10 μM Tris (pH 7.5), 0.4 mM NaN_3, and 0.1 μM excess dendrimer and equilibrated.

DOI: 10.1021/acs.macromol.7b01470
Macromolecules 2017, 50, 8202−8211

Figure 2 shows the time evolution of the measured SAXS scattering profiles for G4-PAMAM−DNA assemblies prepared using lsp and hsp conditions. After condensation, all samples were stored in sealed tubes at room temperature to equilibrate. Figure 2a shows SAXS scattering profiles of lsp G4−DNA taken at 1 h, 3 days, and 6 months. A significant rearrangement of the G4 dendriplex structure is observed over this time scale. Initially, two scattering peaks are observed at short time scales. Inter-DNA spacings are inversely proportional to the scattering vector Q so lower Q reflections correspond to larger DNA−DNA interhelical spacings. Here, the higher Q reflection is seen at $Q \sim 2.09$ nm^{-1}, corresponding to a $D_{Bragg} = 30$ Å. This reflection is comparable to the Bragg spacings previously reported as hexagonal packaging for G4-PAMAM/DNA at pH 8.[17] Interestingly, this spacing is also similar to the hexagonal phase we reported previously for G1-PAMAM/DNA.[25,26] For a hexagonal lattice (Figure 2d), this peak corresponds to an interhelical spacing, D_{int}, of ∼34.6 Å. This 14.6 Å surface separation between DNA helices is significantly smaller than the reported G4 hydrodynamic diameter of 49 Å.[22] Carnerup et al.[22] also observed by TEM that DNA−DNA spacings were nearly constant for DNA condensed by G1 through G4 PAMAM despite the significant difference in the dendrimer size with increasing generation. This suggests a dendrimer deformation is occurring to accommodate the tight DNA packaging. Such deformations of dendrimers interacting with charged surfaces have been experimentally and theoretically observed in other systems.[49,50] The overlap of dendrimers with the DNA cores was also suggested by Evans et al. for G4-PPI/DNA complexes in the square and hexagonal phases where they gave hypothetical arrangements of the DNA and dendrimers that could give rise to both 2D square and hexagonal unit cells.[16] The low q reflection is consistent with previously reported G4−DNA SAXS scattering peaks assigned to both square columnar[17,27] (Figure 2c) and "bead on a string" scattering.[48] Given the fibrous nature of our samples and the high concentration at condensation, we propose this peak is most likely the square columnar phase. The square lattice is characterized by a maximum peak at $Q = 1.57$ nm^{-1}. The interhelical DNA spacing in the square lattice is identical to the Bragg spacing ($D_{Br} = 2\pi/q_{Br}$) and calculated as 40 Å. Over long time periods, this square lattice reflection is lost, and only the hexagonal phase is observed. We did not observe biphasic behavior previously for low generation (G0 and G1) PAMAM/DNA assemblies that formed hexagonal arrays by the lsp method.[25,26] However, this is consistent with other work suggesting higher generation dendrimers condense DNA into trapped states thought to be due to particularly slow interaction kinetics arising from the high surface charge density of the dendrimer.[24,50]

The reorganization of the dendriplex structure with equilibration time in Figure 2a suggests structures that are kinetically trapped states. In an effort to overcome these trapped, nonequilibrium states, we also examined the stability of the G4−DNA assemblies prepared by a high salt preparation (hsp) method. Previously we showed that a hsp method helped circumvent certain kinetic barriers in polyplex structures formed from DNA condensed by high molecular weight linear polycations.[40] The general hypothesis is that lsp may trap precipitates in nonequilibrium states brought about by rapid interaction of the polycation and DNA upon mixing. Once formed, equilibration in these precipitates occurs extremely slowly. Mixing in high salt allows for a thorough mixing of polycation and DNA before precipitation occurs upon dilution. Typical scattering profiles for the hsp method are given in Figure 2b for G4−DNA assemblies. Here, only a single phase is observed with a Bragg reflection occurring at the same Q as the hexagonal phase observed by lsp. The stability of these particles was checked after six months, and no internal spacing rearrangements (<1%) were observed, suggesting a more kinetically stable state has been achieved. Others have previously reported that different packaging is observed for G4−DNA as a function of the nitrogen to phosphate (N/P) charge ratios. Peaks are generally reported to shift to lower Q or equivalently larger inter-DNA spacings with increasing N/P ratio. To examine the effect of charge ratio, we condensed G4−DNA at N/P ranging from 2 to 6 using both the lsp and hsp methods. The fibrous precipitates were subsequently moved to identical equilibration solutions (10 mM Tris, 0.4 mM NaN_3, 0.1 μM G4) and allowed to equilibrate for 2 weeks. For these samples, identical SAXS profiles were observed in G4−DNA for all N/P ratios (Figure S4) made by both methods. We propose that the interior of the dendriplex is charge neutralized upon complete condensation and maintained in the precipitate upon removal from the large excess of free unbound dendrimer in the various N/P formulations. Previously observed structural changes as a function of N/P ratio may suggest that the unbound dendrimer is acting through a salt effect in the low volume X-ray capillaries.

DNA Condensation by zPAMAM with Varying Percent Succinylation. Next, we examined the internal structure of zPAMAM−DNA assemblies with different degrees of succinylation modification to their surface groups. Previously, we measured the intermolecular forces in a variety of linear cation−DNA condensates by using an osmotic stress technique coupled with X-ray scattering. We observed that long-range attractions were dominated by the cation charge, scaling approximately inversely with the cation charge, while the short-range repulsions were dependent on the chemistry of the condensing agent.[41] We also recently showed that the incorporation of a negative moiety into a positively charged polymer surprisingly does not prevent DNA condensation but does alter the resulting DNA packaging.[42] Analysis of the attractive and repulsive forces showed the effect of a negative charge is to dramatically increase the short-range repulsive force, while only slightly reducing the attractive forces, resulting in significantly larger inter-DNA spacings. We hypothesized that the large repulsive force is likely due to the highly unfavorable interactions between the negative residues of the condensing agent being forced in close proximity to the negative DNA phosphates upon binding of the mixed charge peptide in the condensate. Mixed charged systems, therefore, may be used to control DNA packaging.

Our interest here is to determine the resulting supramolecular structure of dendriplexes as a function of the percent succinylation of a series of PAMAM polymers. For ease of comparison, we chose to focus on the more equilibrium structures resulting from zPAMAM−DNA condensed using the high salt preparation method described above. G4 PAMAM has 64 primary amine functional surface groups with only these functional groups charged at neutral pH. With increasing succinylation, the net charge of the zPAMAM is reduced. 0%, 15%, 24%, and 40% zPAMAM would have approximate total charge of +64, +45, +33, and +13, respectively, at neutral pH. All zPAMAMs therefore are expected to be well above the +3 charge threshold for DNA condensation. As expected, more

DOI: 10.1021/acs.macromol.7b01470
Macromolecules 2017, 50, 8202−8211

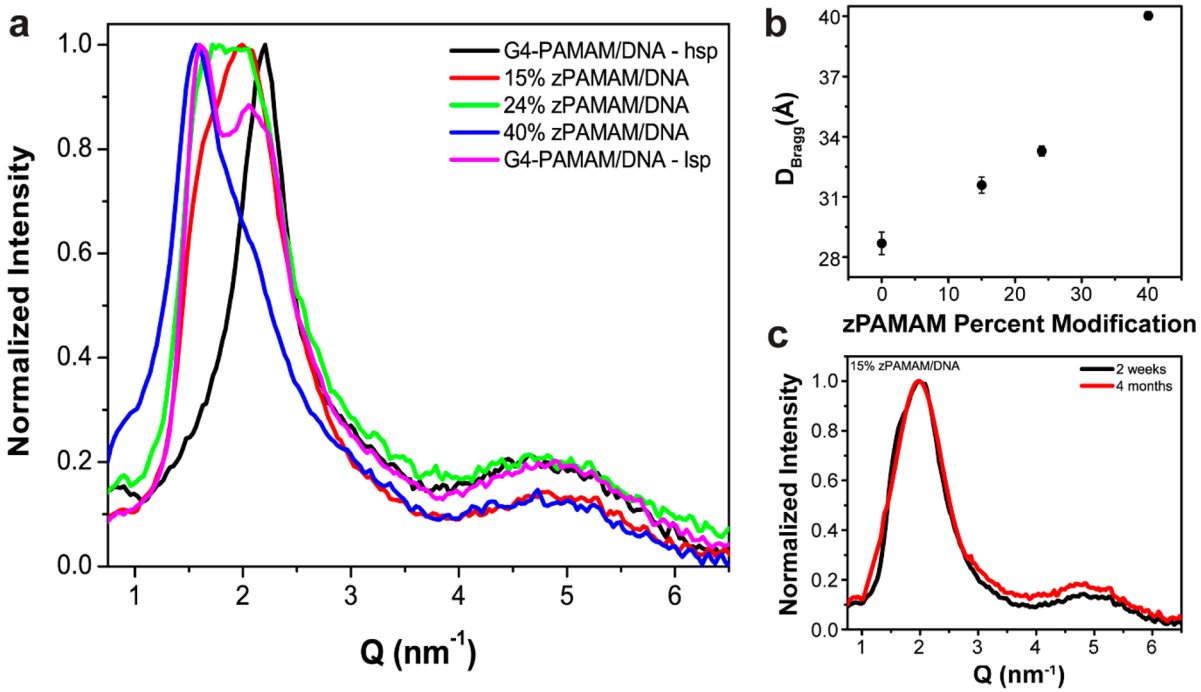

Figure 3. (a) Representative scattering profiles for zPAMAM–DNA. Samples were prepared using the high salt preparation (hsp) equilibrated for 2 weeks in 10 mM Tris (pH 7.5). Data are plotted as the normalized intensity as a function of the scattering vector Q. zPAMAM–DNA complexes show peaks consistent with the columnar square and hexagonal lattices discussed previously for G4–DNA by lsp. At the highest percent modification, zPAMAM preferentially favors the square lattice. For reference, G4–DNA condensed by lsp is also shown. (b) Average calculated D_{Bragg} values for the maximum Bragg peak are plotted as a function of zPAMAM percent modification (c) Scattering profiles for 15% zPAMAM prepared using the hsp after four months do not show significant rearrangement. Higher modifications showed similar long-term stability.

zPAMAM was required to fully condense the DNA compared to G4. The additional zPAMAM required was approximately accounted for by assuming the lower net charge resulting from the degree of succinylation. Shown in Figure 3a are representative normalized scattering profiles for zPAMAM–DNA complexes with the degree of succinylation modification ranging from 0 to 40%. All samples were prepared by the hsp method at pH 7.5 and equilibrated 2 weeks before analysis by SAXS. While unmodified G4–DNA made by hsp resulted in a well-defined single Bragg reflection, increasing the zwitterionic nature of the PAMAM appeared to induce a phase transition to a two-state system. While it is hard to discern the exact nature of this phase transition, it is clear that increased charge modification of the PAMAM primary surface amines results in a significant shift to lower Q or equivalently larger spacings between the DNA helices. The Bragg peak from the maximum scattering peak is plotted in Figure 3b and seen to range from 28.7 to 38.7 Å as the degree of succinylation changes from 0 to 40%. Figure 3c shows 15% zPAMAM prepared from the hsp results in stable structures that did not change over the course of several months. Similar long-term stability was observed for the higher degrees of succinylation zPAMAM–DNA prepared by hsp as well.

In addition to shifting to lower Q, increased succinylation also results in the appearance of a biphasic system with scattering peaks observed at Q values similar to the square and hexagonal phases observed for G4–DNA by the lsp method. 15% zPAMAM–DNA shows a maximum Bragg reflection that is shifted approximately 10% to $Q \sim 2.0$ nm^{-1} compared to G4–DNA. There is also the appearance of an additional weak peak visible as a shoulder at lower Q for this sample. Increasing the percent modification to 24% results in a single but very broad reflection with a significantly higher full width at half-maximum (fwhm) than is typically observed. As shown in Figure 3a, this broad peak nearly perfectly overlaps the two reflections observed in 15% zPAMAM as well as lsp prepared G4–DNA. Most likely this corresponds to an approximately equal distribution of two phases where the high and low Q peaks overlap significantly and are not resolved well. 40% zPAMAM–DNA again shows two distinct peaks but the dominant scattering peak has shifted to the low Q phase. Clearly, degree of modification in zPAMAM allows for the tuning of the dendrimer–DNA interactions and resulting packing densities in the dendriplex assembly. Likely the incorporation of negative charges into PAMAM reduces the total charge on the dendrimer and reduces the interactions with the DNA. This results in a continual shift from the more tightly packaged columnar hexagonal phase to the looser square columnar phase as the dominant equilibrium structure.

Salt Sensitivities of G4–DNA and zPAMAM–DNA Assemblies. A summary of the observed salt sensitivities of the dendrimer–DNA assemblies with increasing added NaCl salt concentration is given in Figure 4. Here all samples were prepared using the hsp method, washed, and equilibrated for 2 weeks in a fresh 10 mM Tris (pH 7.5) bathing solution. The condensate was then transferred to the desired salt–buffer solution and equilibrated for at least 2 days before measurement by SAXS. Figure 4a shows the maximum DNA Bragg spacings for G4–DNA and zPAMAM–DNA condensates as a function of added NaCl concentration. For all dendrimer systems, added NaCl salt causes the DNA packaging to swell, resulting in larger DNA–DNA spacings. Focusing first on unmodified G4–DNA, we observe a systematic shift to larger with increasing salt concentration up to 600 mM NaCl.

DOI: 10.1021/acs.macromol.7b01470
Macromolecules 2017, 50, 8202–8211

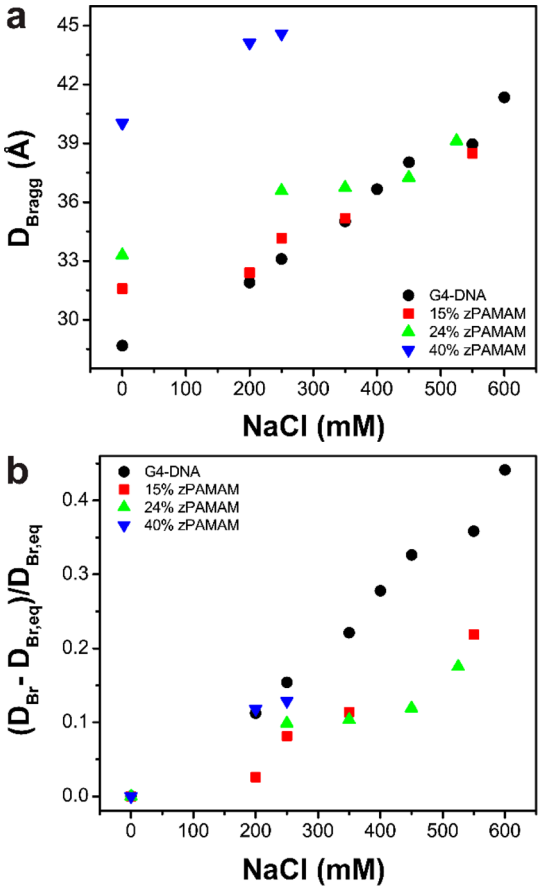

Figure 4. Salt effects on G4-PAMAM/DNA and zPAMAM/DNA complexes (a) Bragg spacing (D_{Br}) dependence as a function of added NaCl concentration for DNA condensed by unmodified and zwitterionic G4-PAMAM. The equilibrium solutions show no Bragg scattering at the next higher salt concentration in each series. (b) Relative change in the Bragg spacing for G4−DNA and zPAMAM−DNA assemblies as a function of added NaCl concentration. The slope is related to the rate of swelling in these different systems.

Equilibrium Bragg spacings (D_{Br}) increase from approximately 28.7 Å to 41.3 Å over this salt range. We previously showed in a linear cation−DNA system that the addition of salt does not simply screen electrostatic attractions in the condensed DNA phase. Instead, the swelling observed is the result of a complicated combination of electrostatic screening, anion binding to the bound cation, and/or cation competition with the bound cation for DNA binding and is highly dependent on the salt species.[51] By 650 mM added NaCl salt concentration, G4−DNA samples completely lose any Bragg scattering such that no reflections are observed. Where scattering is lost is most likely indicative of either complete dissolution of the sample or formation of an isotropic network of DNA and PAMAM polymer. For unmodified G4−DNA, we also compared swelling behavior for samples made by either the high salt or low salt (hsp vs lsp) methods (Figure S5). Comparison of the hexagonal phases observed by both methods showed that with increasing salt concentration, the observed Bragg spacings are nearly identical. This indicates the salt sensitivity of the hexagonal phase is independent of the sample preparation method.

We next examined the effect of zPAMAM on the salt sensitivities of the resulting dendriplexes. We hypothesized that the incorporation of negative moieties into the PAMAM will not only give rise to the observed larger Bragg spacings but also affect the sensitivity of zPAMAM to salt. For all systems, added NaCl salt causes the DNA packaging to swell resulting in larger inter-DNA spacings (Figure 4). Higher succinylation weakens the dendrimer−DNA interactions and leads to less stable dendriplexes. The critical salt concentration at which no Bragg scattering is observed decreases systematically. 15% and 24% zPAMAM show no Bragg scattering between 550 and 600 mM NaCl. 40% zPAMAM-DNA shows no Bragg scattering by 300 mM NaCl. In Figure 4b, we plot the relative change in the Bragg spacing $[(D_{Br} - D_{Br,eq})/D_{Br,eq}]$ as a function of the added NaCl concentration. $D_{Br,eq}$ is the equilibrium Bragg spacing observed for the dendriplexes without added salt. The percent zwitterionic nature of the dendrimer does not play a significant role in the rate of the swelling, as indicated by the slope in Figure 4; however, the percent swelling varies slightly with degree of PAMAM modification. Inter-DNA spacings for G4−DNA swells over 40% compared to only 10−20% swelling for the zPAMAM−DNA systems. This corresponds to an increase in D_{Br} of ∼13 Å for G4−DNA but only ∼5−6 Å for the zPAMAM−DNA condensates studied before Bragg scattering is lost.

Role of pH on G4-PAMAM/DNA and zPAMAM/DNA Packaging. pH plays a significant role in changing the observed DNA packaging for dendriplexes. PAMAM dendrimers consist of both primary and tertiary amines with different pK_a values. PAMAM molecules will thus carry different net charges at different pH.[52,53] G4-PAMAM has 64 primary amines at the outer surface of the dendrimer and an additional 62 tertiary amine at the branch points. At near neutral pH, all the primary amine groups are fully charged while the tertiary branch amines carry almost no charge.[52] Lowering the pH further increases the PAMAM charge due to protonation of the tertiary amines. For pH at or above ∼8, primary amines can be deprotonated, thereby decreasing the net charge. Here, we focus on determining the role of pH at condensation on the resulting inter-DNA spacings for G4−DNA and zPAMAM−DNA complexes. DNA and dendrimer from stock solutions were buffered to the desired pH values (pH 4−8) with HCl or NaOH. Buffers used were 10 mM sodium acetate solution for pH 4, 10 mM MES solution for pH 6, and 10 mM Tris-HCl for pH 7.5−8. DNA was subsequently precipitated with the pH buffered dendrimer using the high or low salt preparation methods. Samples were equilibrated for 2 weeks in fresh pH buffered aqueous solution with a slight excess (0.1 μM) of dendrimer.

Figure 5a,b shows the normalized scattering profile curves and calculated Bragg spacings of the hsp prepared G4−DNA assemblies condensed at different pH. With decreasing pH, the Bragg peak is observed to shift to higher Q or equivalently smaller DNA−DNA spacings. At pH 4, Q = 2.38 nm^{-1}, while at pH 8, Q = 1.94 nm^{-1}. This corresponds to Bragg spacings ranging from 26.4 to 32.4 Å. At pH 8, there is a significant increase in the full width at half-maximum of the Bragg reflection compared to the lower pH samples. This may indicate a biphasic state where the deprotonation of some surface amines has resulted in the formation of a high population of a more loosely ordered state. At pH 4, some tertiary amines of the PAMAM become charged, increasing the net dendrimer charge. In these samples, we see not only a shift to higher Q, or equivalently smaller inter-DNA spacings, but also a decrease in the FWHM of the peak, suggesting a more compact phase with better long-range ordering. Similar shifts in

DOI: 10.1021/acs.macromol.7b01470
Macromolecules 2017, 50, 8202−8211

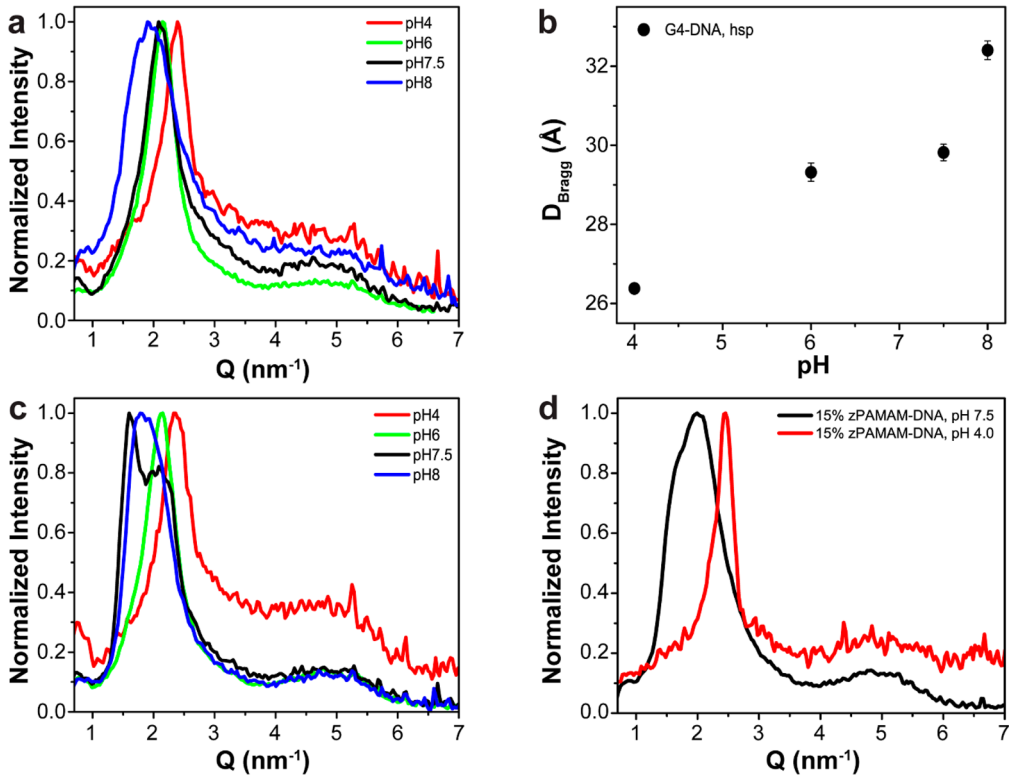

Figure 5. pH effects on DNA packaging in G4−DNA and zPAMAM−DNA. (a) Normalized scattering profiles of G4−DNA condensed at different pH using the high salt preparation (hsp) method. (b) Measured D_{Bragg} reflection as a function of pH from hsp. (c) Normalized scattering profiles of G4-PAMAM condensed at different pHs using the low salt preparation (lsp) method. (d) Representative scattering profiles of 15% zPAMAM−DNA condensed at low and high pH.

the scattering profiles were observed for G4−DNA made by the lsp method (Figure 5c). Scattering profiles show a characteristic shift to lower Q with increasing pH ranging from $Q \sim 2.36$ nm^{-1} to $Q \sim 1.63$ nm^{-1} for the maximum Bragg reflection. Again, at pH 8, there is a significant increase in the FWHM. This broad peak is nearly overlapping the biphasic scattering profile observed at pH 7.5, suggestive of a biphasic (square and hexagonal) system in both samples. At lower pH, only one Bragg reflection is observed, consistent with a hexagonal lattice that shifts to lower Q with decreasing pH. Once condensed, changing the pH buffer also induces similar shifts in the equilibrium DNA spacing, but the magnitude of the shift is decreased. We previously reported similar results in low generation (G0/G1) PAMAM−DNA complexes.[25] We proposed this is due to the pK_as of bound PAMAM amines being shifted in the condensate and their ability to protonate or deprotonate are different than PAMAM in free solution.

zPAMAM−DNA packaging was also observed to be sensitive to the pH as shown in Figure 4d. Here we show 15% zPAMAM condensed at either pH 7.5 or pH 4. The low pH leads to a significantly tighter DNA packaging as evidenced by the large shift to higher Q. In addition, the peak width is significantly narrower at low pH, consistent with the presence of only a single phase, the columnar hexagonal, being present in these samples. This tighter packaging is likely due to the increased net charge of the low pH zPAMAM dendrimer due to charging of the tertiary amines, thus increasing the dendrimer−DNA interactions significantly. Changing the pH for intermediate generation dendrimers is thought to affect the dendrimer radius of gyration[52] which may also explain some of the pH dependence in the observed packaging densities.

CONCLUSIONS

We have investigated the structure of DNA condensates resulting from self-assembly of DNA with fourth-generation PAMAM and zPAMAM dendrimers. Inter-DNA spacings are observed to be highly dependent on the degree of succinylation. Evidence for a phase transition between hexagonal and square columnar phase is also observed at high degrees of dendrimer modification. Salt sensitivities and pH dependence of the PAMAM and zPAMAM dendriplexes were also examined. Higher degrees of succinylation reduce polymer−DNA interactions resulting in less stable DNA condensates. Increasing the charge by lowering pH results in stronger dendrimer−DNA interactions leading to significantly tighter DNA packaging. The ability to tune dendrimer−DNA interactions through postsynthesis modifications is an attractive means to engineer effective gene delivery vectors as well as new tools for binding DNA for biological and biomedical applications. The zPAMAM systems should also benefit from highly reduced cellular toxicity due to the reduced net charge and zwitterionic nature of the dendrimer. We are currently investigating the potential of zPAMAM as a tunable nucleic acid delivery vector.

ASSOCIATED CONTENT

Supporting Information

The Supporting Information is available free of charge on the ACS Publications website at DOI: 10.1021/acs.macromol.7b01470.

SI 1−3: detailed description of zPAMAM synthesis and ^{1}H NMR characterization of 40, 24, and 15%

DOI: 10.1021/acs.macromol.7b01470
Macromolecules 2017, 50, 8202−8211

succinylated zPAMAM; SI 4: details regarding the scattering data collected to examine the effects of mixing nitrogen to phosphate (N/P) ratios using the low and high salt preparation methods; SI 5: additional scattering data collected in this study and the D_{Bragg} values extracted from peak fitting of salt effects on high and low salt preparation methods on unmodified G4-PAMAM (PDF)

AUTHOR INFORMATION

Corresponding Author

*E-mail derouchey@uky.edu; phone (859) 323-2827; fax (859) 323-9985 (J.E.D.).

ORCID

Vincent M. Rotello: 0000-0002-5184-5439

Jason E. DeRouchey: 0000-0002-3624-4432

Present Address

M.A.: Department of Clinical Microbiology and Immunology of Southwest Hospital and the College of Medical Laboratory Science, Third Military Medical University, Chongqing, China.

Notes

The authors declare no competing financial interest.

ACKNOWLEDGMENTS

J.E.D. acknowledges financial support from the National Science Foundation (MCB-1453168). J.E.D. and M.A. acknowledges support from the University of Kentucky Research Challenge Trust Fund (RCTF) Fellowship for Biochemistry. V.M.R. acknowledges support from the NIH (GM077173).

REFERENCES

(1) Eisenberg, T.; Knauer, H.; Schauer, A.; Buttner, S.; Ruckenstuhl, C.; Carmona-Gutierrez, D.; Ring, J.; Schroeder, S.; Magnes, C.; Antonacci, L.; Fussi, H.; Deszcz, L.; Hartl, R.; Schraml, E.; Criollo, A.; Megalou, E.; Weiskopf, D.; Laun, P.; Heeren, G.; Breitenbach, M.; Grubeck-Loebenstein, B.; Herker, E.; Fahrenkrog, B.; Frohlich, K.-U.; Sinner, F.; Tavernarakis, N.; Minois, N.; Kroemer, G.; Madeo, F. Induction of autophagy by spermidine promotes longevity. *Nat. Cell Biol.* **2009**, *11* (11), 1305−1314.

(2) Wong, G. C.; Pollack, L. Electrostatics of strongly charged biological polymers: ion-mediated interactions and self-organization in nucleic acids and proteins. *Annu. Rev. Phys. Chem.* **2010**, *61*, 171−89.

(3) Yoo, J.; Aksimentiev, A. The structure and intermolecular forces of DNA condensates. *Nucleic Acids Res.* **2016**, *44* (5), 2036−46.

(4) Dekker, J.; Marti-Renom, M. A.; Mirny, L. A. Exploring the three-dimensional organization of genomes: interpreting chromatin interaction data. *Nat. Rev. Genet.* **2013**, *14* (6), 390−403.

(5) Knobler, C. M.; Gelbart, W. M. Physical chemistry of DNA viruses. *Annu. Rev. Phys. Chem.* **2009**, *60*, 367−83.

(6) Pack, D. W.; Hoffman, A. S.; Pun, S.; Stayton, P. S. Design and development of polymers for gene delivery. *Nat. Rev. Drug Discovery* **2005**, *4* (7), 581−593.

(7) Yin, H.; Kanasty, R. L.; Eltoukhy, A. A.; Vegas, A. J.; Dorkin, J. R.; Anderson, D. G. Non-viral vectors for gene-based therapy. *Nat. Rev. Genet.* **2014**, *15* (8), 541−555.

(8) Ziebarth, J.; Wang, Y. Molecular dynamics simulations of DNA-polycation complex formation. *Biophys. J.* **2009**, *97* (7), 1971−83.

(9) Wagner, K.; Harries, D.; May, S.; Kahl, V.; Rädler, J. O.; Ben-Shaul, A. Direct Evidence for Counterion Release upon Cationic Lipid−DNA Condensation. *Langmuir* **2000**, *16* (2), 303−306.

(10) Mascotti, D. P.; Lohman, T. M. Thermodynamic extent of counterion release upon binding oligolysines to single-stranded nucleic acids. *Proc. Natl. Acad. Sci. U. S. A.* **1990**, *87* (8), 3142−6.

(11) Merdan, T.; Kopecek, J.; Kissel, T. Prospects for cationic polymers in gene and oligonucleotide therapy against cancer. *Adv. Drug Delivery Rev.* **2002**, *54* (5), 715−58.

(12) Morille, M.; Passirani, C.; Vonarbourg, A.; Clavreul, A.; Benoit, J.-P. Progress in developing cationic vectors for non-viral systemic gene therapy against cancer. *Biomaterials* **2008**, *29* (24), 3477−3496.

(13) Wagner, E. Polymers for nucleic acid transfer-an overview. *Adv. Genet.* **2014**, *88*, 231−61.

(14) Bielinska, A. U.; Chen, C.; Johnson, J.; Baker, J. R. DNA Complexing with Polyamidoamine Dendrimers: Implications for Transfection. *Bioconjugate Chem.* **1999**, *10* (5), 843−850.

(15) Dufes, C.; Uchegbu, I. F.; Schatzlein, A. G. Dendrimers in gene delivery. *Adv. Drug Delivery Rev.* **2005**, *57* (15), 2177−202.

(16) Evans, H. M.; Ahmad, A.; Ewert, K.; Pfohl, T.; Martin-Herranz, A.; Bruinsma, R. F.; Safinya, C. R. Structural polymorphism of DNA-dendrimer complexes. *Phys. Rev. Lett.* **2003**, *91* (7), 075501.

(17) Liu, Y.-C.; Chen, H.-L.; Su, C.-J.; Lin, H.-K.; Liu, W.-L.; Jeng, U. S. Mesomorphic Complexes of Poly(amidoamine) Dendrimer with DNA. *Macromolecules* **2005**, *38* (23), 9434−9440.

(18) Dootz, R.; Otten, A.; Köster, S.; Struth, B.; Pfohl, T. Evolution of DNA compaction in microchannels. *J. Phys.: Condens. Matter* **2006**, *18* (18), S639.

(19) Pfohl, T.; Otten, A.; Köster, S.; Dootz, R.; Struth, B.; Evans, H. M. Highly Packed and Oriented DNA Mesophases Identified Using in Situ Microfluidic X-ray Microdiffraction. *Biomacromolecules* **2007**, *8* (7), 2167−2172.

(20) Su, C.-J.; Chen, H.-L.; Wei, M.-C.; Peng, S.-F.; Sung, H.-W.; Ivanov, V. A. Columnar Mesophases of the Complexes of DNA with Low-Generation Poly(amido amine) Dendrimers. *Biomacromolecules* **2009**, *10* (4), 773−783.

(21) Ainalem, M.-L.; Nylander, T. DNA condensation using cationic dendrimers-morphology and supramolecular structure of formed aggregates. *Soft Matter* **2011**, *7* (10), 4577−4594.

(22) Carnerup, A. M.; Ainalem, M.-L.; Alfredsson, V.; Nylander, T. Condensation of DNA using poly(amido amine) dendrimers: effect of salt concentration on aggregate morphology. *Soft Matter* **2011**, *7* (2), 760−768.

(23) Chen, C.-Y.; Su, C.-J.; Peng, S.-F.; Chen, H.-L.; Sung, H.-W. Dendrimer-induced DNA bending. *Soft Matter* **2011**, *7* (1), 61−63.

(24) Dootz, R.; Toma, A. C.; Pfohl, T. PAMAM6 dendrimers and DNA: pH dependent "beads-on-a-string" behavior revealed by small angle X-ray scattering. *Soft Matter* **2011**, *7* (18), 8343−8351.

(25) An, M.; Hutchison, J. M.; Parkin, S. R.; DeRouchey, J. E. Role of pH on the Compaction Energies and Phase Behavior of Low Generation PAMAM−DNA Complexes. *Macromolecules* **2014**, *47* (24), 8768−8776.

(26) An, M.; Parkin, S. R.; DeRouchey, J. E. Intermolecular forces between low generation PAMAM dendrimer condensed DNA helices: role of cation architecture. *Soft Matter* **2014**, *10* (4), 590−599.

(27) Schmidt, N. W.; Jin, F.; Lande, R.; Curk, T.; Xian, W.; Lee, C.; Frasca, L.; Frenkel, D.; Dobnikar, J.; Gilliet, M.; Wong, G. C. L. Liquid-crystalline ordering of antimicrobial peptide-DNA complexes controls TLR9 activation. *Nat. Mater.* **2015**, *14* (7), 696−700.

(28) Huang, Y.-C.; Su, C.-J.; Chen, C.-Y.; Chen, H.-L.; Jeng, U. S.; Berezhnoy, N. V.; Nordenskiöld, L.; Ivanov, V. A. Elucidating the DNA−Histone Interaction in Nucleosome from the DNA−Dendrimer Complex. *Macromolecules* **2016**, *49* (11), 4277−4285.

(29) Su, C.-J.; Chen, C.-Y.; Lin, M.-C.; Chen, H.-L.; Iwase, H.; Koizumi, S.; Hashimoto, T. Nucleosome-like Structure from Dendrimer-Induced DNA Compaction. *Macromolecules* **2012**, *45* (12), 5208−5217.

(30) Peng, S. F.; Su, C. J.; Wei, M. C.; Chen, C. Y.; Liao, Z. X.; Lee, P. W.; Chen, H. L.; Sung, H. W. Effects of the nanostructure of dendrimer/DNA complexes on their endocytosis and gene expression. *Biomaterials* **2010**, *31* (21), 5660−70.

(31) Kukowska-Latallo, J. F.; Bielinska, A. U.; Johnson, J.; Spindler, R.; Tomalia, D. A.; Baker, J. R., Jr. Efficient transfer of genetic material into mammalian cells using Starburst polyamidoamine dendrimers. *Proc. Natl. Acad. Sci. U. S. A.* **1996**, *93* (10), 4897−902.

DOI: 10.1021/acs.macromol.7b01470
Macromolecules 2017, 50, 8202−8211

(32) Morille, M.; Passirani, C.; Vonarbourg, A.; Clavreul, A.; Benoit, J. P. Progress in developing cationic vectors for non-viral systemic gene therapy against cancer. *Biomaterials* **2008**, *29* (24−25), 3477−96.
(33) Kolhatkar, R. B.; Kitchens, K. M.; Swaan, P. W.; Ghandehari, H. Surface Acetylation of Polyamidoamine (PAMAM) Dendrimers Decreases Cytotoxicity while Maintaining Membrane Permeability. *Bioconjugate Chem.* **2007**, *18* (6), 2054−2060.
(34) McGhee, J. D.; Wood, W. I.; Dolan, M.; Engel, J. D.; Felsenfeld, G. A 200 base pair region at the 5′ end of the chicken adult beta-globin gene is accessible to nuclease digestion. *Cell* **1981**, *27* (1), 45−55.
(35) van Dongen, M. A.; Orr, B. G.; Banaszak Holl, M. M. Diffusion NMR Study of Generation-Five PAMAM Dendrimer Materials. *J. Phys. Chem. B* **2014**, *118* (25), 7195−7202.
(36) Bloomfield, V. A. DNA condensation by multivalent cations. *Biopolymers* **1997**, *44* (3), 269−82.
(37) Rau, D. C.; Parsegian, V. A. Direct measurement of the intermolecular forces between counterion-condensed DNA double helices. Evidence for long range attractive hydration forces. *Biophys. J.* **1992**, *61* (1), 246−259.
(38) Todd, B. A.; Adrian Parsegian, V.; Shirahata, A.; Thomas, T. J.; Rau, D. C. Attractive Forces between Cation Condensed DNA Double Helices. *Biophys. J.* **2008**, *94* (12), 4775−4782.
(39) DeRouchey, J.; Hoover, B.; Rau, D. C. A Comparison of DNA Compaction by Arginine and Lysine Peptides: A Physical Basis for Arginine Rich Protamines. *Biochemistry* **2013**, *52* (17), 3000−3009.
(40) DeRouchey, J.; Netz, R. R.; Radler, J. O. Structural investigations of DNA-polycation complexes. *Eur. Phys. J. E: Soft Matter Biol. Phys.* **2005**, *16* (1), 17−28.
(41) DeRouchey, J.; Parsegian, V. A.; Rau, D. C. Cation Charge Dependence of the Forces Driving DNA Assembly. *Biophys. J.* **2010**, *99* (8), 2608−2615.
(42) DeRouchey, J. E.; Rau, D. C. Role of amino acid insertions on intermolecular forces between arginine peptide condensed DNA helices: implications for protamine-DNA packaging in sperm. *J. Biol. Chem.* **2011**, *286* (49), 41985−41992.
(43) Golan, R.; Pietrasanta, L. I.; Hsieh, W.; Hansma, H. G. DNA Toroids: Stages in Condensation. *Biochemistry* **1999**, *38* (42), 14069−14076.
(44) Martin, A. L.; Davies, M. C.; Rackstraw, B. J.; Roberts, C. J.; Stolnik, S.; Tendler, S. J. B.; Williams, P. M. Observation of DNA−polymer condensate formation in real time at a molecular level. *FEBS Lett.* **2000**, *480* (2−3), 106−112.
(45) Balhorn, R.; Brewer, L.; Corzett, M. DNA condensation by protamine and arginine-rich peptides: Analysis of toroid stability using single DNA molecules. *Mol. Reprod. Dev.* **2000**, *56* (S2), 230−234.
(46) Kunze, K. K.; Netz, R. R. Salt-Induced DNA-Histone Complexation. *Phys. Rev. Lett.* **2000**, *85* (20), 4389−4392.
(47) Nguyen, T. T.; Shklovskii, B. I. Complexation of DNA with positive spheres: Phase diagram of charge inversion and reentrant condensation. *J. Chem. Phys.* **2001**, *115* (15), 7298−7308.
(48) Yang, C. C.; Huang, Y. C.; Chen, C. Y.; Su, C. J.; Chen, H. L.; Ivanov, V. A. Structure of the Electrostatic Complex of DNA with Cationic Dendrimer of Intermediate Generation: The Role of Counterion Entropy. *Macromolecules* **2014**, *47* (9), 3117−3127.
(49) Ainalem, M.-L.; Bartles, A.; Muck, J.; Dias, R. S.; Carnerup, A. M.; Zink, D.; Nylander, T. DNA Compaction Induced by a Cationic Polymer or Surfactant Impact Gene Expression and DNA Degradation. *PLoS One* **2014**, *9* (3), e92692.
(50) Ainalem, M.-L.; Campbell, R. A.; Nylander, T. Interactions between DNA and Poly(amido amine) Dendrimers on Silica Surfaces. *Langmuir* **2010**, *26* (11), 8625−8635.
(51) DeRouchey, J. E.; Rau, D. C. Salt Effects on Condensed Protamine-DNA Assemblies: Anion Binding and Weakening of Attraction. *J. Phys. Chem. B* **2011**, *115* (41), 11888−11894.
(52) Maiti, P. K.; Çağın, T.; Lin, S.-T.; Goddard, W. A. Effect of Solvent and pH on the Structure of PAMAM Dendrimers. *Macromolecules* **2005**, *38* (3), 979−991.
(53) Welch, P.; Muthukumar, M. Tuning the Density Profile of Dendritic Polyelectrolytes. *Macromolecules* **1998**, *31* (17), 5892−5897.

DOI: 10.1021/acs.macromol.7b01470
Macromolecules 2017, 50, 8202−8211